Combining controlled-source seismology and local earthquake tomography to derive a 3-D crustal model of the western Alpine region

Michael Wagner,[1] Edi Kissling[2] and Stephan Husen[1]

[1] *Swiss Seismological Service, Swiss Federal Institute of Technology, ETH Zurich, CH-8092, Switzerland. E-mail: wagner@sed.ethz.ch*
[2] *Institute of Geophysics, Swiss Federal Institute of Technology, ETH Zurich, CH-8092, Switzerland*

SUMMARY

We present a newly developed approach of combining controlled-source seismology (CSS) and local earthquake tomography (LET) data to obtain a new 3-D crustal model of the western Alpine region. Our approach combines either data by taking into account the strengths of the individual seismic methods. Our western Alpine 3-D model is primarily based on a well-defined Moho, constrained by CSS and LET data, and includes smooth lateral variations in seismic velocities mainly constrained by LET data, but locally also by CSS data. The consistent combination of results from the two different seismic methods is feasible due to LET Moho elements, as defined by characteristic *P*-wave velocities and their uncertainty estimates. These uncertainty estimates are based on values of the diagonal element of the resolution matrix, absolute *P*-wave velocities that are typical for crust and mantle and a specific velocity gradient across the Moho discontinuity. Finally, our definition of LET Moho elements and their uncertainties is validated by comparisons of highest quality Moho results from both methods coinciding in 353 localities. Our model clearly shows three Moho surfaces, being Europe, Adria and Liguria as well as major tectonic structures like suture zones and the high-velocity Ivrea body. In general, it is in a good agreement with previous studies. The biggest differences occur along plate boundaries, where the strong lateral velocity variations are best resolved by LET. Due to the larger number of available Moho reflector elements a more accurate definition of plate boundaries at Moho level is possible and, therefore, new insights in deep lithosphere structures of the Alpine collision zone can be expected. Furthermore, our new 3-D crustal model directly includes a 3-D migrated image of the Ivrea body.

Key words: Controlled-source seismology; Seismic tomography; Crustal structure; Europe.

GJI Seismology

1 INTRODUCTION

Refraction and reflection seismology, both controlled-source seismology (CSS) methods, are complementary high-resolution imaging techniques (e.g. Banda & Mooney 1982). They have provided a wealth of information on crustal structure worldwide, and, in particular, on the crustal structure of the Alpine region (e.g. Kissling *et al.* 2006). CSS methods are especially suitable for detecting and imaging seismic interfaces showing a strong contrast in seismic velocity, such as the crust–mantle boundary (Moho).

On the crustal scale, CSS methods are 2-D techniques applied to 3-D structures. Controlled sources are either at or close to the Earth's surface. This leads to an imaging geometry with sources and receivers on the same side of the studied volume. Knowing the seismic velocities, it is possible to determine depth, and approximate location and dip of a reflecting/refracting element. This process is

called 2-D (in-line) migration and is routinely applied along 2-D seismic profiles. Using the information from several crossing 2-D seismic profiles the 2-D (in-line) migration can be further constrained and subsequently allows a 3-D (off-line) migration of the reflector elements (e.g. Kissling *et al.* 1997; Waldhauser *et al.* 1998). Due to the setup of CSS methods (source–receiver geometry) and considering the resulting ray paths, however, which are often more or less parallel to each other, information obtained on seismic velocities is limited. Furthermore, due to the CSS source–receiver geometry in combination with the inherent nature of seismic wave energy being preferably transmitted by high-velocity low-attenuation rock volumes, CSS-derived seismic models exhibit a tendency towards the higher velocities, while smaller low-velocity zones remain unsampled (Kissling 1993).

The simultaneous inversion for hypocentre locations and 3-D seismic velocity structure is known as local earthquake tomography

(LET; e.g. Thurber 1983; Kissling 1988). LET can provide 3-D images of seismic velocities of the lithosphere with a spatial resolution up to a few kilometres (e.g. Eberhart-Phillips 1993). The parametrization of LET models, in combination with less certain phase identification (when compared to CSS) in 3-D cases, however, hampers precise tomographic imaging of sharp geological boundaries, that is, seismic first-order discontinuities. In contrast with this limitation is the very good resolution of 3-D volumetric velocities due to favourable geometry of sources and receivers and the resulting 3-D crossing of rays. Moreover, tomography is a true 3-D method with source and receiver at different sides of the study volume and, hence, no migration is needed.

Several attempts have been made to obtain a crustal model satisfying data from both CSS and LET methods. One attempt relies on the so-called 'minimum 1-D model' that acts as the optimal initial 1-D model to the 3-D LET inversion (Kissling *et al.* 1994). In the process of computing a minimum 1-D model, layering of the 1-D model is usually constrained by CSS data. Thus, through the minimum 1-D model *a priori* information from CSS is included into the LET inversion process of the coupled hypocentre-velocity model problem.

Treating shots as earthquakes with a fixed location in LET has been proposed, for example, by Miller & Smith (1999). However, when only first arriving phases are included in the tomography no improved constraints on deep seismic discontinuities can be obtained. Nevertheless, resolution of near-surface structures is usually improved.

Applying a different approach, Husen *et al.* (2003) used the 3-D CSS *P*-wave velocity model of Waldhauser *et al.* (2002) as an initial reference model for their LET model of Switzerland. The fine (6 km × 6 km × 2 km) model parametrization of the CSS model (Waldhauser *et al.* 1998) had to be enlarged to fit the ray coverage of the earthquake data to avoid inversion instabilities in LET. In the final model, LET well-resolved regions are mainly constrained by LET data, whereas poorly resolved regions, such as the Moho or the shallow subsurface, are mainly constrained by *a priori* CSS data. Still, this model represents rather an LET model without strong velocity discontinuities using CSS information as *a priori* constraints.

A more realistic 3-D crustal model that includes strong velocity discontinuities and realistic 3-D variations in seismic velocities, can be obtained by simultaneously combining data from both methods and, thereby, preserving the strength of each method. Therefore, we propose a procedure to extract information on the Moho depth out of the LET model and combine this information with Moho depths derived from CSS data. Knowing the exact geometry of the Moho discontinuity is very important for several seismic applications. The earthquake hypocentre determination, for example, can benefit from including secondary (e.g. Moho reflected) phases. Based on a well-defined Moho topography, a crustal model is established using all crustal velocity information from CSS and LET. Thus, taking into account the above-mentioned strengths of the individual seismic methods and combining them to largely eliminate the drawbacks of the other seismic methods will result in a 3-D crustal model that is consistent with CSS and LET data and that overcomes the limitations of previous crustal models. Recent efforts in crustal structure imaging (Waldhauser *et al.* 2002; Husen *et al.* 2003; Diehl *et al.* 2009a) make the greater western Alpine region an ideal place to develop such a model that will also help to further improve our understanding of the highly complex tectonics in the region (Schmid *et al.* 2004).

2 HIGH-QUALITY CSS AND LET DATA SETS IN THE ALPINE REGION

2.1 CSS data

In the greater western Alpine region over 250 CSS near-vertical reflection and refraction profiles exist (e.g. Kissling *et al.* 2006). Along these profiles the Moho discontinuity is sampled by means of reflector elements in a discrete fashion (Fig. 1). Weighting of each reflector element is based on a number of quality factors (Ansorge & Baumann 1997; Kissling *et al.* 1997; Waldhauser *et al.* 1998). For wide-angle seismic reflection and refraction profiles these include raw data quality or phase confidence (w_c), orientation of the profile relative to the 3-D tectonic settings (w_o) and profile type or ray coverage (w_t). Reflector elements of near-vertical seismic reflection profiles are quality weighted based on reflectivity signature (w_{cr}), migration criteria (w_{mig}) and projection distance (w_{proj}; Holliger & Kissling 1991). Total weighting factors (w_{tot}) were obtained by multiplying the individual weights for refraction and reflection data:

$$w_{tot} = w_c \cdot w_o \cdot w_t \tag{1a}$$

and

$$w_{tot} = w_{cr} \cdot w_{mig} \cdot w_{proj}, \tag{1b}$$

respectively.

They range between 0.1 (information poorly constrained by CSS methods) and 1.0 (highly reliable reflectors from CSS methods). Total weight of each reflector element is related to the error in depth for an optimal case by considering the Fresnel volume for a very well-resolved reflector element (Baumann 1994; Kissling *et al.* 1997). Considering the Fresnel volume for an average frequency content of 6 Hz for Moho reflections from active sources and an average Alpine Moho depth of 40 km, a vertical resolution ($frsn_{err}$) of ±3 km is derived for the best case ($w_{tot} = 1.0$). Therefore, the
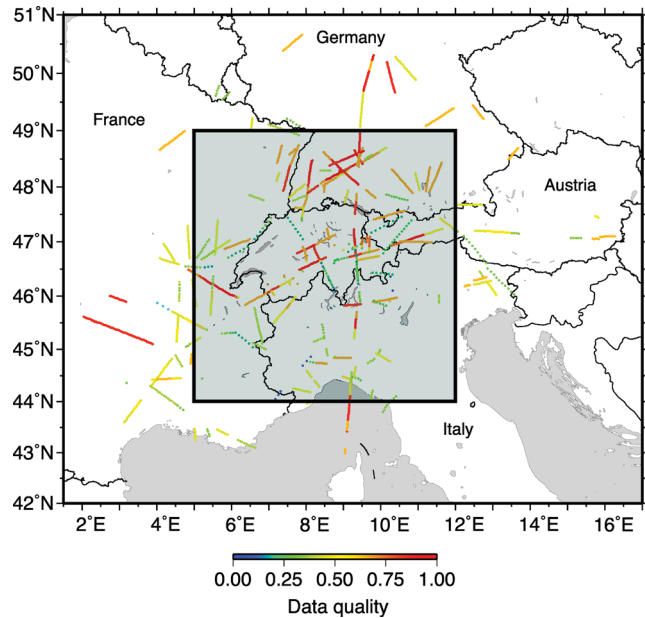
Figure 1. Migrated CSS Moho reflector elements for the Alpine region (after Waldhauser *et al.* 2002). Each reflector element is colour coded based on the total weighting factor (data quality) ranging from 0.1 (poorly constrained) to 1.0 (well constrained). Grey shaded area shows model region in this study.

weight-dependent depth uncertainty (z_{err}) is estimated as:

$$z_{err} = \frac{frsn_{err}}{w_{tot}}$$
$$= \frac{\pm 3 \text{ km}}{w_{tot}}. \tag{2}$$

Waldhauser *et al.* (1998, 2002) used these reflector elements to model the Moho topography that is based on considerations of roughness and continuity, that is, it is searched for the smoothest and simplest interface that still fits the data within their uncertainties and has the highest continuity. After interpolation of the 1- or 2-D (in-line) migrated reflector elements and separation into three Moho surfaces, being Europe, Adria and Liguria, the reflector elements were 3-D (off-line) migrated and again interpolated for final Moho topography.

2.2 LET data

Using arrival time data from local earthquakes, the crustal structure of the greater Alpine region has been imaged in the past by LET (e.g. Solarino *et al.* 1997; Husen *et al.* 2003; Béthoux *et al.* 2007; Diehl *et al.* 2009a; Di Stefano *et al.* 2009). Solarino *et al.* (1997) used routine traveltime picks from different agencies. While the Ivrea body was well documented, inconsistencies in routine picks limited the resolution of Moho topography. For lack of waveform data, Di Stefano *et al.* (2009) also used traveltime picks from different agencies for their northern model part, resulting in similar resolution problems. Husen *et al.* (2003) and Béthoux *et al.* (2007) only resolved relatively small parts of our study area. Thus, in this study we use the tomographic model of Diehl *et al.* (2009a) to derive LET Moho elements, because it is the newest and most complete tomographic model for that region and it was developed using consistent and high-quality data (Diehl *et al.* 2009b).

The model of Diehl *et al.* (2009a) is based on more than 13 000 high-quality first-arriving *Pg* and *Pn* phases from 552 well-locatable local earthquakes in the greater Alpine region that were recorded at about 400 stations (Diehl *et al.* 2009b). Waveforms for these events were compiled from archives of 11 local, regional and national seismological observatories. Arrival times were re-picked using an automated quality-weighted approach (Aldersons 2004; Di Stefano *et al.* 2006; Diehl *et al.* 2009b). The coupled hypocentre-velocity problem was solved by a linearized simultaneous inversion for hypocentre locations and 3-D *P*-wave velocity structure. The resulting model parametrization of 25 km × 25 km (horizontal) × 15 km (vertical) for the central part of their model provided the best possible parametrization concerning cell size, ray coverage and model resolution (Diehl *et al.* 2009a). The solution quality of the tomographic model was assessed using tests with synthetic data in comparison with the resolution matrix (Diehl *et al.* 2009a). These tests showed that regions associated with an RDE larger than 0.15 are fairly well resolved and larger than 0.3 are very well resolved. These well-resolved parts of the model document over a wide area seismic velocities of the upper crust, as well as the lower crust and the crust–mantle boundary (Moho) that are especially important for our purpose.

3 3-D MODELLING OF COMBINED CSS AND LET DATA

Our approach to combine CSS and LET data is based on several principles like, for example (i) the knowledge of Moho data of different seismic methods and related uncertainties, (ii) the understanding of how the different methods sample the Moho and assess uncertainties of specific Moho elements in relation to optimal experimental setup and (iii) the principle of simplicity in respect to Moho surface interpolation that is defined by interface continuity and roughness (Waldhauser *et al.* 1998). For each seismic data, we first derive Moho elements that define the location and depth of the Moho. These Moho elements are the centrepiece of our approach, because they form the base for the interpolation of the Moho surface(s). Mapping the Moho by individual results from different seismic methods means also that we need to know the individual uncertainties and possible 3-D migration needs of each Moho element. The individual uncertainty of every Moho element must be consistent within each method and reflect its possibilities in mapping the Moho discontinuity.

3.1 LET Moho elements

In contrast to CSS data, local earthquake data do not sample the Moho discontinuity by means of discrete reflector/refractor elements (Waldhauser *et al.* 1998). Rather, LET provides a continuous image of the 3-D subsurface velocity field based on more or less smooth variations of volumetric averaged seismic velocities sampled on a regular or irregular grid. Limitations in minimal cell size, as well as the fact that only first arriving phases are commonly used for LET, hamper imaging of first-order discontinuities, such as the Moho. In case of the Moho, however, geological, petrological and geophysical considerations about seismic velocities of the lower crust and the upper mantle allow the interpretation of a rather smooth velocity field in terms of this well-known first-order velocity discontinuity. On the basis of a test with a synthetic velocity model that was derived from a 3-D CSS velocity model for the Alpine region (Waldhauser *et al.* 1998, 2002), Diehl *et al.* (2009a) found a good agreement between Moho depth and the 7.25 km s^{-1} *P*-wave velocity contour line for their tomographic model of the Alpine region (fig. 8 in Diehl *et al.* 2009a). In regions of good solution quality, we use this velocity as a first-order indicator to define LET Moho elements.

In LET, seismic velocities represent averaged velocities of cells with a vertical extension up to several kilometres. In the LET study by Diehl *et al.* (2009a) that was used to build our crustal model, the vertical cell dimensions are 15 km. This means that the LET model is a gradient velocity model, defined at seismic grid points (25 km × 25 km × 15 km). Due to this vertical cell dimension the velocity gradient across the Moho is fairly weak, which results in a seemingly rather untypical velocity value of 7.25 km s^{-1} for the identification of the Moho. In addition, however, the Moho is characterized by specific velocities of the lower crust and uppermost mantle, as well as a characteristic gradient between the crust and mantle. *P*-wave velocities in the European continental lower crust are typically less than 6.5 km s^{-1} (Mueller 1977). Below the Moho discontinuity *P*-wave velocities are typically larger than 8.0 km s^{-1} (e.g. peridotite: 8.1 km s^{-1}; Mueller 1977; Christensen 1996; Mooney *et al.* 1998). As a consequence, seismic velocities at gridpoints above the Moho discontinuity (Vp_a) and below the Moho discontinuity (Vp_c) need to show clear crustal and mantle velocities (Fig. 2).

An additional criterion for the identification of LET Moho elements is a strong velocity gradient across the LET Moho (7.25 km s^{-1} contour line) that is typical for the transition from crust into mantle and that can be resolved with the above-mentioned vertical extension of the LET model cells of 15 km. For a clear identification of the Moho, it is requested that the *P*-wave velocity 4 km above
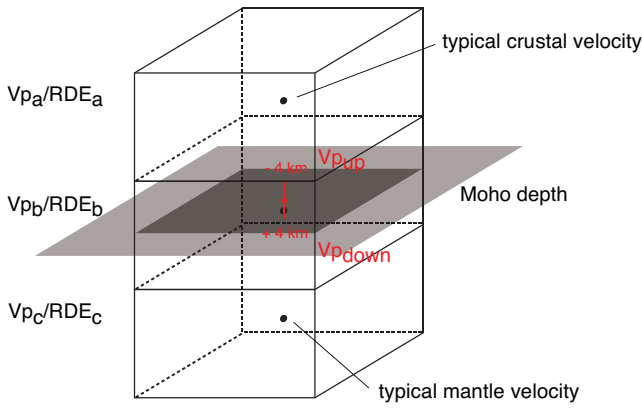
Figure 2. Definition of LET grid nodes (black dots) and cells and their respective *P*-wave velocities and RDE values used for determination of LET Moho element uncertainty classes. *P*-wave velocity and RDE value of the grid nodes closest to the Moho are assigned to Vp_b and RDE_b, respectively. Velocities and RDE values of grid nodes above and below the Moho are assigned to Vp_a and RDE_a, and Vp_c and RDE_c, respectively. Vp_{up} and Vp_{down} are *P*-wave velocities 4 km above and 4 km below the calculated Moho depth marked by red dot, respectively. See text for more details on how these parameters are used to define LET uncertainty classes.

the Moho is lower than 6.9 km s^{-1} (Vp_{up}) and that it is greater than 7.6 km s^{-1} (Vp_{down}) 4 km below the Moho (Fig. 2). These specific values have been obtained by careful calibration of the above-mentioned principles to the LET results of Diehl *et al.* (2009a). For the definition of top class (class 0) LET Moho elements all these criteria must be fulfilled (Table 1).

3.2 LET Moho element uncertainties

To allow consistent merging with CSS Moho reflector elements (Fig. 1), LET Moho elements must be weighted according to their uncertainty in a similar fashion as it is done for CSS Moho reflector elements (Kissling *et al.* 1997; Waldhauser *et al.* 1998). In our approach, LET uncertainty classes are based on RDE values (Husen *et al.* 2000) and absolute *P*-wave velocities of the different model cells, as well as the *P*-wave velocity gradient around the Moho discontinuity (Table 1). The diagonal element of the resolution matrix (RDE) is used as a measure for ray coverage defining resolution

capabilities. Model parameters that are constrained by a large number of rays with different orientations can be considered as well resolved (e.g. Eberhart-Phillips 1990). To use the RDE as a quality factor, it needs to be calibrated by a series of tests with different synthetic models (e.g. Haslinger *et al.* 1999). For the LET model used in this study, an RDE value larger than 0.15 is considered to define well-resolved model parameters (Diehl *et al.* 2009a). As the solution quality of a single model parameter may also depend on the solution quality of its neighbours (Kissling 1988; Reyners *et al.* 1999; Kissling & Husen 2001) we use information on the RDE not only of the cell containing the LET Moho elements, but also of its neighbours (Fig. 2).

Based on this strategy, three classes are defined to asses the uncertainty of individual LET Moho elements (Table 1). Class 0 is characterized by a triplet (above, at Moho and below) of very well-imaged LET cells (RDE $\geq 2 \times 0.15$) and matching all specific velocity requests, that is, absolute values above and below Moho and velocity gradient across Moho. Then, the error in depth is limited to an estimated Fresnel volume of ± 5 km considering a frequency content of 2 Hz for Moho depths between 20 and 40 km, similar to the values obtained for CSS error estimates (Kissling *et al.* 1997). For class 1 reliable imaging (RDE ≥ 0.15) of velocity information in this region is required for cells above, at and below the Moho. If either the requirements on absolute velocity information or velocity gradient information are fulfilled, the above-mentioned vertical cell size of 15 km is responsible for an error in depth of ± 7 km. In all other cases, LET Moho elements are assigned to class 2 and not used further in this study.

3.3 Consistency in CSS and LET Moho data

For each LET Moho element, we compute the depth to the 7.25 km s^{-1} velocity isosurface in the LET model of Diehl *et al.* (2009a). As previously discussed a *P*-wave velocity of 7.25 km s^{-1} represents,

Table 2. Number of all LET Moho elements assigned to class 0 and class 1 and those of class 0 and class 1 who are consistent with CSS Moho reflector elements weighted between 0.2 and 1.0.

Criterion	Class 0	Class 1	Total
All	420	2332	2752
$\Delta z \leq err_{LET} + err_{CSS}$	71	278	349
$\Delta z > err_{LET} + err_{CSS}$	0	4	4

Table 1. Configuration of the LET uncertainty classes. RDE values ensure a good resolution of the velocities in the model cells. LET Moho elements are weighted based on the absolute velocities at the gridpoints above (Vp_a) and below (Vp_c) the Moho and the velocity gradient ± 4 km around the Moho depth (Vp_{up}, Vp_{down}) (class 0). For class 1 LET Moho elements either absolute velocity values or velocity gradient must apply. Note the difference in requested RDE values between class 0 and class 1. For a description of RDE and Vp see Fig. 2 and text. z_a is the depth of the gridpoint belonging to RDE_a and Vp_a, respectively.

Class	RDE	Vp_{abs} (km s^{-1})	Vp_{grad} (km s^{-1})	Resulting uncertainty (km)
		and		
0	$RDE_a \geq 2\,RDE_{min}$ $RDE_b \geq 2\,RDE_{min}$ $RDE_c \geq 2\,RDE_{min}$	$Vp_a > 6.0$ if $z_a > 25$ km $Vp_a < 6.5$ $Vp_c > 7.8$	$Vp_{up} < 6.9$ $Vp_{down} > 7.6$	± 5
		either/or		
1	$RDE_a \geq RDE_{min}$ $RDE_b \geq RDE_{min}$ $RDE_c \geq RDE_{min}$	$Vp_a > 6.0$ if $z_a > 25$ km $Vp_a < 6.5$ $Vp_c > 7.8$	$Vp_{up} < 6.9$ $Vp_{down} > 7.6$	± 7
2		else		rejected

as a first-order approximation, the Moho in our model. The computation is done on a regular 6 km × 6 km (horizontal) grid, as defined by the desired resolution for Moho interface modelling (Waldhauser *et al.* 1998). The extraction of LET Moho elements and association with a Moho surface is done automatically. Uncertainty estimates

(quality classes) of the elements are calculated and assigned as defined by Table 1. In total we find 2752 Moho elements, thereof 420 in class 0 and 2332 in class 1 (Table 2 and Fig. 4). Furthermore, 353 LET Moho elements have a corresponding CSS Moho reflector element, allowing to test Moho depth and uncertainty estimates by
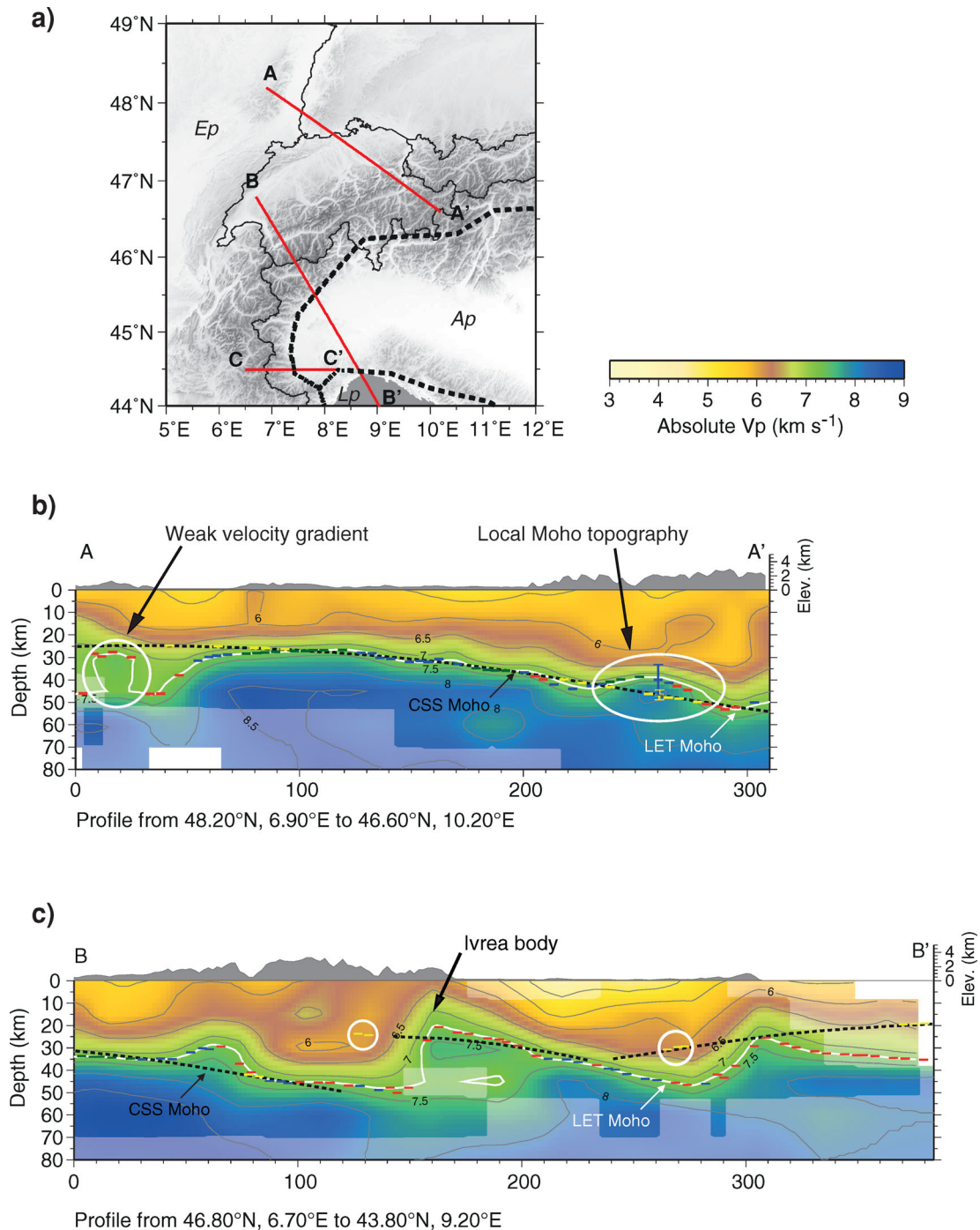
Figure 3. (a) Orientation of profiles shown here and in Fig. 5. Dashed black lines mark plate boundaries between European, Adriatic and Ligurian plates. (b, c) Vertical cross-sections through 3-D LET model. Thin white contour line marks 7.25 km s^{-1} velocity. Dashed black line shows the Moho depth after Waldhauser *et al.* (1998). Bars symbolize the Moho reflector elements: CSS weight 0.2–1.0 (yellow), LET class 0 (green), LET class 1 (blue) and LET class 2 (red). Shaded colours outline areas of insufficient resolution. Areas with very poor ray coverage are shown in white. (b) The area between 10 and 50 km along the profile shows the importance of the LET uncertainty class criterion based on velocity gradients above and below Moho (see text). The white ellipsoid centred at 260 km along profile marks an area of local Moho topography that is not seen in CSS due to sparse data and simplicity. Error bars of a CSS and LET Moho element in this area are shown exemplarily. (c) The white circles highlight the wrongly identified and migrated CSS Moho reflector elements that are responsible for great differences in CSS and LET Moho depth (see Fig. 4 and Appendix A).
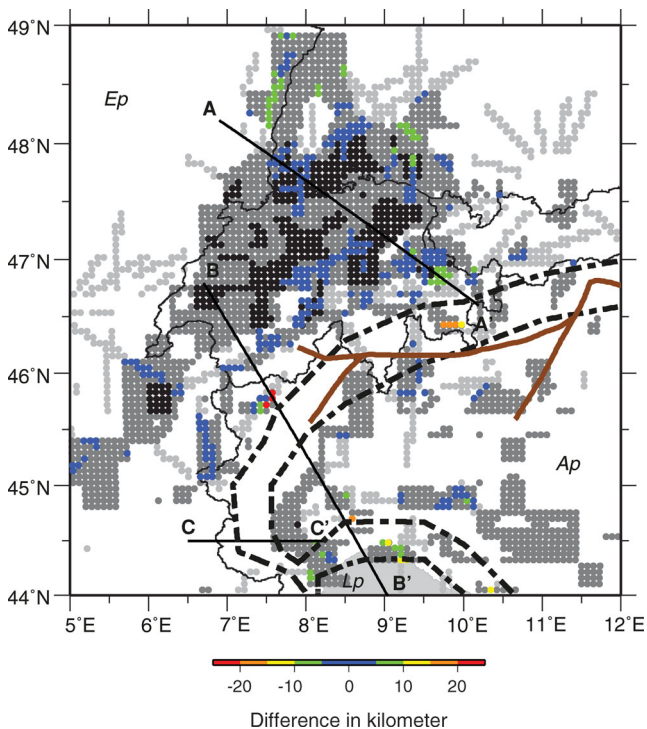
Figure 4. Dots symbolize CSS and LET Moho reflector elements. Black: LET Moho elements of class 0. Dark grey: LET Moho elements of class 1. Light grey: CSS Moho reflector elements. Coloured: difference in depth (km) of CSS Moho reflector elements weighted between 0.2 and 1.0 and LET Moho elements of class 0 and class 1. Black dashed line shows areas (polygons) for automatic extraction and association of LET Moho elements (Ep: European Plate, Ap: Adriatic Plate, Lp: Ligurian Plate). Brown line shows schematic alignment of Insubric Line. Profiles AA' and BB' are shown in Fig. 3; profile CC' in Fig. 5. Note that co-located CSS and LET Moho elements showing a significant mismatch (yellow–orange–red) are exclusively found along plate boundaries.

comparison of CSS and LET results. For 349 LET Moho elements, the sum of estimated depth uncertainty is smaller than or equal to the difference in Moho depth (Fig. 4). Of these 349 LET Moho elements, 71 elements belong to LET error class 0 and 278 elements to class 1 (Table 2). We find only four elements of class 1 (Table 2 and Figs 3 and 4) for which the difference in Moho depth is greater than the error sum of the uncertainty estimates (see also Appendices A and B). These are all located close to plate boundaries and demonstrate that in such regions a manual extraction and association of Moho elements must be performed (see Appendix C). After manual extraction and association, no nearby elements with Moho depth difference greater than the error sum of their uncertainty estimates remain in our data set. This demonstrates the consistency of the proposed procedure to extract Moho depth from LET and CSS information.

3.4 Preparation of Moho reflector elements for interpolation

In the interpolation process the weight attributed to an individual Moho element is inversely proportional to its uncertainty estimate. The weight is represented by the number of points (segment points) within the Fresnel volume width (Waldhauser *et al.* 1998). Fig. 6(a) shows the distribution of segment points between starting point and endpoint of a CSS Moho reflector element with $w_{tot} = 1.0$ that is

equivalent to an uncertainty in Moho depth of ±3 km. In this case (top quality) a CSS segment point defines an area of 8 km².

The equivalent distribution of segment points for LET data within LET uncertainty class 0 and class 1, and their associated approximated Fresnel volume, is presented in Fig. 6(b). In contrast to CSS, model parametrization in LET is defined by 3-D cells, which requires a 2-D distribution of segment points for the Moho interpolation. Thus, for the interpolation process, LET Moho elements are extracted on the original LET seismic grid (25 km × 25 km horizontally) and not on the 6 km × 6 km horizontally spaced grid that was used for the comparison with CSS Moho reflector elements (Fig. 4). This area of 625 km², defined by the horizontal extension of an LET cell, has to be represented by LET segment points to be consistent with CSS definition. The LET segment point distribution considers the related error in depth for class 0 (±5 km) and class 1 (±7 km) LET Moho elements in comparison to CSS depth errors. In addition, for LET Moho elements there should be more weight given to the centre (gridpoint) of each cell. Consequently, weights for LET Moho elements will be represented by 32 and 16 segment points for LET class 0 and class 1, respectively. Similar to CSS these LET Moho segment points reflect the trend in Moho depth on their underlying surface. An overview of the available CSS and LET Moho data used for interpolation is shown in Fig. 7.

3.5 Moho surface interpolation of combined CSS and LET data

Once all LET Moho elements and associated quality classes have been defined, they may easily be merged with the CSS Moho reflector elements to proceed to the interpolation of the Moho surfaces. The procedure is described in detail in Waldhauser (1996) and Waldhauser *et al.* (1998) for modelling of the Moho interface based on CSS information only.

As our study area is denoted by three Moho surfaces separated by offsets at plate boundaries, we seek after the simplest surface for each individual Moho. In this context, simplicity means that it is searched for the smoothest and most continuous Moho surface that satisfies all LET and CSS Moho reflector elements within their uncertainties (Waldhauser *et al.* 1998). Since the original CSS Moho reflector elements are not migrated in 3-D, a first interpolation through all CSS and LET Moho elements must be performed to obtain a surface for 3-D migration of the CSS Moho reflector elements. After 3-D migration of all CSS Moho reflector elements, a second interpolation is performed to obtain the final Moho surfaces.

4 RESULTS

The results of the interpolation through the combined CSS and LET data set are shown in Fig. 8. Our new 3-D crustal model in the western Alpine region extends from 44°N, 5°E to 49°N, 12°E. In this region the Moho depth ranges between 10–16 km (Ivrea) and 60 km (mountain root below the central Alps) below sea level. Fig. 8(b) shows a 3-D perspective view on the Moho topography, looking from northeast. The model clearly shows three Moho interfaces being Europe, Adria and Liguria with the Moho offsets to fulfill the requirements of smoothness and simplicity in interface modelling (Waldhauser *et al.* 1998).

As can already be seen from these figures, our study area is a region of tectonically high complexity with several plate boundaries and a dominant high-velocity zone (Ivrea). The European Moho is
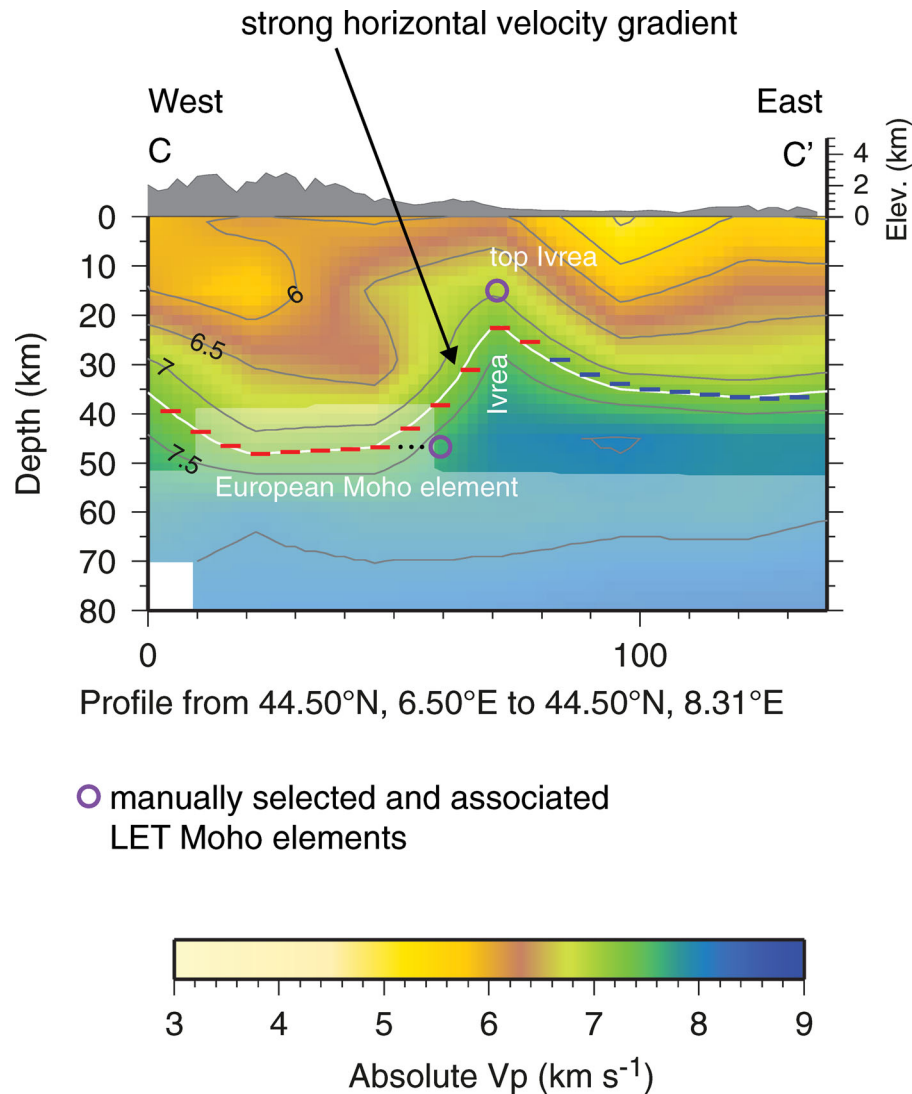
Figure 5. Vertical cross-section through 3-D LET model of Diehl *et al.* (2009a) illustrating how LET Moho elements were manually identified and associated with a specific Moho interface (for location of profile see Fig. 3 and/or Fig. 4). Bars show automatically extracted LET Moho elements (red: class 2, blue: class 1). Class 2 LET Moho elements are not used in this study. Purple circles show manually extracted and associated LET Moho elements. The deep-seated western Moho element is associated with the European Moho, while the shallow and eastern element on top of Ivrea mantle is associated with the Adriatic Moho (see text).

southward dipping from about 28 km below the northern foreland to about 60 km below the Insubric Line in the central Alps. In the western Alps the Moho dips eastwards (Fig. 8).

The Adriatic Moho shows a complex structure reflecting the recent tectonic evolution of the microplate. Northwards, it is imaged with a depth of about 40 km, overthrusting the European Moho. At the southern rim it reaches depths of around 56 km and, therefore, underthrusting the Ligurian Moho. In between it is shallowing to normal depths of about 30 km along an E–W-trending axis paralleling the centre of the Po plain. Towards the west the Adriatic Moho clearly marks the top of the Ivrea body regionally shallowing to depths of 16 km and locally to even less (Fig. 8).

The Ligurian Moho is smoothly changing in depth from a minimum of about 16 km beneath the deepest parts of the Ligurian Sea to 28 km in the north and west towards the northern Apennines (Fig. 8). In contrast to the Moho offset between the Ligurian and Adriatic Moho in the northern Apennines, the transition between the European and the Ligurian Moho in the eastern part is very smooth at a depth around 28 km.

5 DISCUSSION

Combining data from complementary CSS and LET methods and, thus, taking advantage of the strength of each method is an excellent possibility to develop 3-D crustal models. Pursuing this approach means to use the Moho discontinuity as a common denominator. While CSS is inherently useful to image the Moho discontinuity, LET Moho information is derived from LET velocities. Hence, if we establish a Moho topography in accordance with CSS and LET information, the crustal velocities mapped by LET combined with this Moho represents the best initial 3-D crustal model.

Uncertainty estimates of LET data work well for automated Moho element extraction. With the requested resolution quality

a)

b)
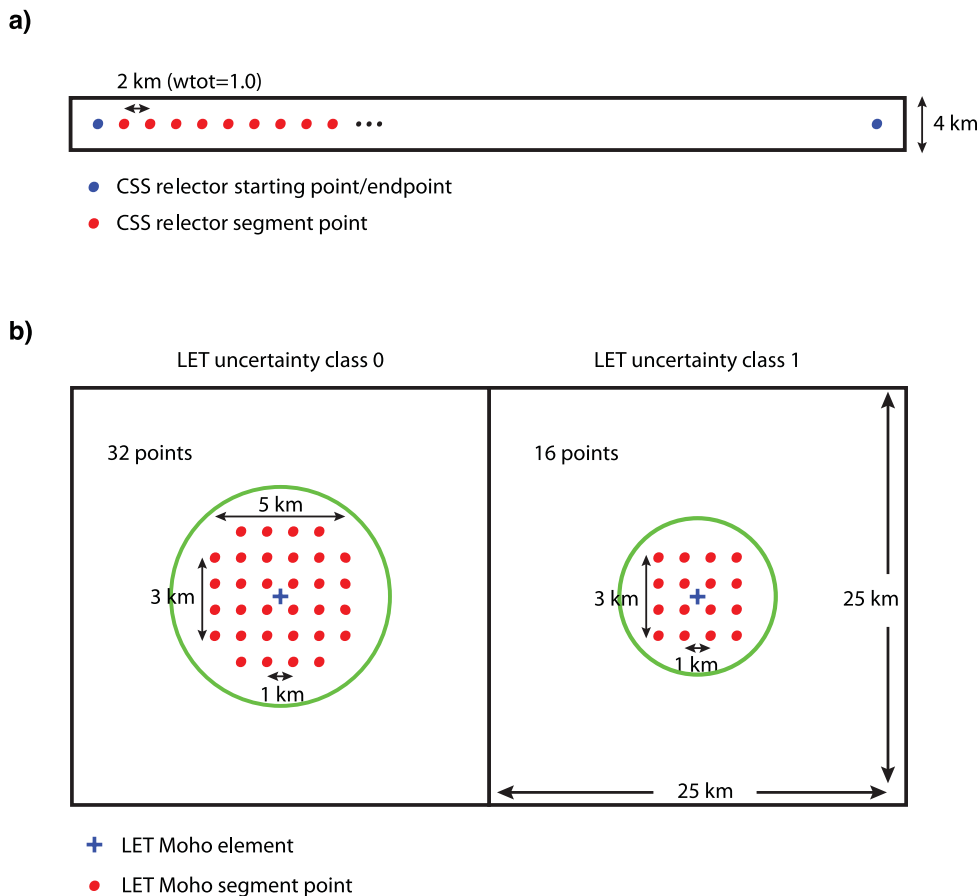
Figure 6. Moho elements are translated into a number of segment points according to quality of information and distributed over a region defined by resolution power of seismic method. (a) Definition of CSS reflector segment points used for interpolation. (b) Definition of LET Moho segment points used for interpolation and schematic illustration of the associated approximated Fresnel volume (green circle). For more details see text.

(see Table 1) these estimates might be on the conservative side. We deliberately chose this scheme of rather high-resolution requests for the automated Moho extraction since the uncertainty of poorly resolved points is difficult to asses and, therefore, blunders may not be excluded. If needed, additional LET Moho elements and associated uncertainties might always be extracted manually (see Appendix C).

The overall good correlation between our improved 3-D crustal model and the model of Waldhauser *et al.* (1998) is shown along profile 1, the European Geotraverse (EGT; Blundell *et al.* 1992, Fig. 9a), where a good coverage by CSS and LET data exists. Along this profile Moho topography was already exceptionally well constrained by CSS data (Kissling *et al.* 2006). While the Moho topography does not change along this profile, the new additional LET data significantly enhances the internal crustal structure. The most important improvements of our new model, however, are evident in regions, where CSS information alone is too sparse to resolve detailed Moho topography and, in particular, at plate boundaries and close to the Ivrea body (Fig. 9b), where 3-D migration of CSS Moho reflector elements is often uncertain.

Along the EGT (Blundell *et al.* 1992) the European Moho is imaged at approximately 28–30 km depth in the northern Alpine foreland (Fig. 9a). Beneath the northernmost central Alps the Moho descends rapidly and almost reaches 60 km beneath the southern Alps, where it underthrusts the Adriatic Moho forming the Alpine crustal root. The Adriatic Moho, on the other hand, is bending upwards beneath the Po plain and underthrusting the Ligurian Plate towards south. Beneath the northernmost Apennines there exists a large Moho offset of about 30 km between the Adriatic Moho at 56 km and the shallower Ligurian Moho, well documented by LET and CSS data. Further south, however, the LET information by Diehl *et al.* (2009a) is less reliable than the CSS information along the EGT profile that shows a further shallowing towards the Ligurian Sea to about 20 km depth. The three different Moho's are separated by two significant vertical offsets marking the plate boundaries between Europe, Adria and Liguria.

The profile across the western Alps (Profile 2, Fig. 9b) again shows the three Moho's distinctively separated and, in addition, the high-velocity Ivrea body that is constituted by peridotitic rocks of upper-mantle origin (Schmid 1967, 1968). The Ivrea zone with its adjacent lower crustal continental rocks has been used as a model for continental crust and Moho (Schmid *et al.* 2004). For this cross-section, Schmid & Kissling (2000) presented a structural model based on CSS, geological and gravimetric information, as well as a comparison with independent tomographic information by So-larino *et al.* (1997). Their cross-section is in general accordance with Diehl *et al.* (2009a) and with our Moho interpretation. With only very few and poorly constrained CSS reflector elements in this area, however, the trend of the Adriatic Moho as upper bounds of the Ivrea body had to be extrapolated by Schmid & Kissling (2000). Often, in cases like the Ivrea body or at convergent plate boundaries, and, in particular, in collision zones like the Alps, where the
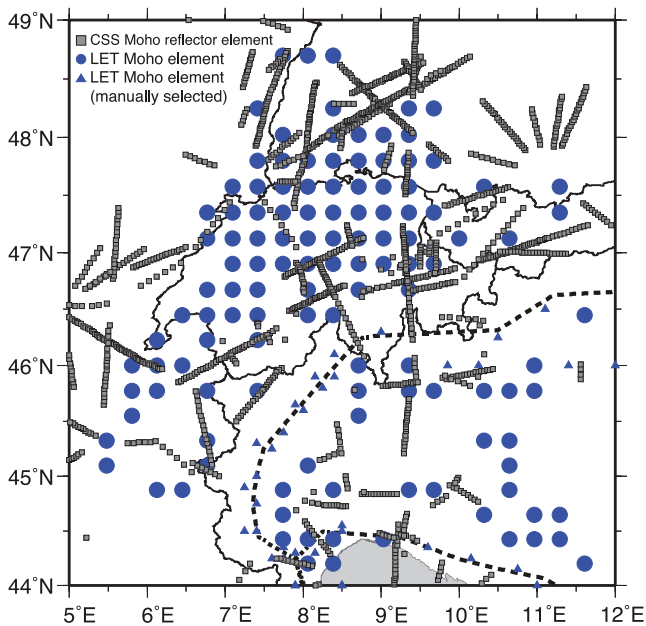
Figure 7. Compiled LET and CSS Moho data used for Moho surface interpolation in this study. Blue dots symbolize automatically determined LET Moho information. Blue triangles show manually selected LET Moho elements outside of polygons for automatic association (close to plate boundaries). Grey squares show (migrated) CSS Moho reflector elements as compiled by Waldhauser *et al.* (2002).

structures are mostly subvertical, they are too steep to be well constrained by CSS methods (Kissling 1993; Solarino *et al.* 1997). With our additional LET Moho information it is now possible to clearly identify and model the geometry of the Adriatic Moho and to further track the European Plate underthrusting the Ivrea body (Fig. 9b). To the southeast the Adriatic Moho is descending down to about 50 km towards the plate boundary with Liguria. Similar to the plate boundary across Ivrea, the boundary between Adria and Liguria shifted significantly when compared to the model of Waldhauser *et al.* (1998, Fig. 9b). This further documents the improvements in our new 3-D crustal model based on CSS and LET data in relation to the model of Waldhauser *et al.* (2002) that relied solely on CSS information and where the Ivrea body was only *a posteriori* included based on Solarino *et al.* (1997).

As mentioned above, various approaches have been previously proposed to combine CSS and receiver function (RF) data, as well as LET and CSS data for crustal structure modelling. Di Stefano *et al.* (2011) followed the same philosophy as Waldhauser *et al.* (1998) when using CSS data for the Moho interpolation. In addition, they exploited RF information to further constrain the Moho depth. Their RF data, however, lack a consistent uncertainty estimation in respect to CSS information and with only a few more Moho points in our study region, the complex Moho topography could not be resolved significantly better than Waldhauser *et al.* (1998).

Husen *et al.* (2003) employed a CSS-based initial reference model in their LET. Due to limited resolution power of their LET data, the *a priori* CSS Moho topography had to be parametrized as a step function on a rather coarse LET grid. In the study of Husen *et al.* (2003), mainly earthquakes within Switzerland and, thus, only a few *Pn* phases were used. This significantly reduces the resolution power of LET data at depths below 40 km and, hence, the initial model remains unaltered, which is nicely seen in Fig. 10(a). Whereas

crustal structure is locally improved, CSS information alone does not help to improve Moho topography in the LET model.

On the other hand, the LET model of Diehl *et al.* (2009a) that was used in our study, includes a large number of *Pn* phases from earthquakes covering the greater Alpine region. Thus, ray coverage and resolution power of the LET data at greater depths are much higher than in the model of Husen *et al.* (2003). Diehl *et al.* (2009a) used a minimum 1-D model as initial model for the 3-D inversion process. The resolution of mid-crustal structures in the central Alps is only marginally better than the one in the model of Husen *et al.* (2003), but the resolution of Moho topography is significantly better. As the Moho topography can be identified based on criteria for velocities and velocity gradients, it is consistent with our combined CSS and LET Moho (Fig. 10b).

The difference in Moho topography in the models of Husen *et al.* (2003), Diehl *et al.* (2009a) and the results in this study document the improved approach of determining crustal models based on different seismic methods. Instead of directly using data from CSS and LET methods in a combined way, the strategy of Husen *et al.* (2003) was to employ CSS model results as an initial model for the inversion of LET data. On the contrary, in our approach we perform an approximated coupled inversion of both CSS and LET data. This means, we interpolate the Moho depth by simultaneously fitting CSS and LET data within their uncertainty estimates. In fact, our result clearly shows that crustal models satisfying high-quality data sets from both seismic methods are best determined by using the strengths of either method in an approximated coupled inversion and not by applying results of one method as *a priori* constraints for the other method.

6 CONCLUSION

Due to the large amount of CSS data (see, e.g. Waldhauser *et al.* 1998, and references therein) and several LET studies (e.g. Solarino *et al.* 1997; Husen *et al.* 2003; Béthoux *et al.* 2007; Diehl *et al.* 2009a), the western Alpine region is the perfect place to develop a new 3-D crustal model based on those two complementary seismic methods by employing each of their individual strengths. Following the pre-defined approach of combining CSS and LET information (Section 3) we showed their consistency concerning the Moho topography (see Fig. 4 and Table 2) once the Moho is identified in the LET model. Definition of the LET Moho follows strict rules that allow automated extraction of Moho depth and uncertainty estimates. Care must be taken in areas of highly complex velocity structures, such as convergent plate boundaries, where an automatic approach is neither useful nor reasonable. In these regions careful manual checking of vertical cross-sections, however, is very successful (Appendices B and C). Based on this strategy, high-quality 3-D LET Moho information can be obtained and, in combination with CSS data, used to compile improved 3-D crustal models.

Our improved 3-D crustal model in the western Alpine region is generally in good agreement with earlier models like, for example, the model of Waldhauser *et al.* (1998), based on CSS data only, as well as the model of Diehl *et al.* (2009a) that is derived from LET data only. Due to 3-D migration needs, a CSS only derived model is often ambiguous in regions of high complexity as, for example, at plate boundaries and close to the Ivrea body. Thanks to the additional LET Moho elements complementing the previously existing CSS information, our new model is more reliable and precise than the previous ones. Thus, the larger number of Moho reflector
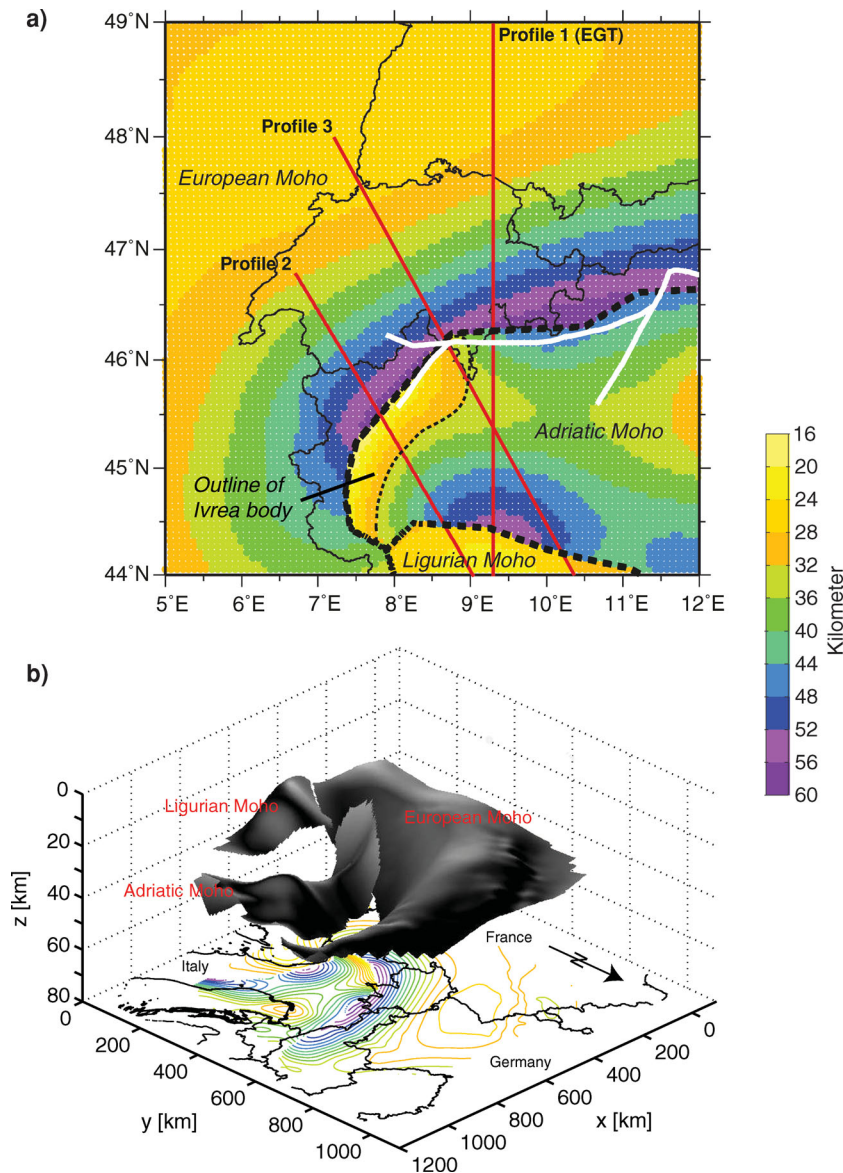
Figure 8. (a) Depth of the western Alpine Moho derived from interpolation of combined CSS and LET data. Dashed thick black line marks the plate boundaries between European, Adriatic and Ligurian plates. Dashed thin black line shows outline of the Ivrea body. Red lines show orientation of profiles in Section 5. White line shows schematic alignment of Insubric Line. (b) Perspective view from the northeast on the Moho topography of the western Alpine region including 2 km spaced coloured contour lines of the Moho depth.

elements (e.g. Fig. 4) allows for a more accurate definition of the plate boundaries and a precise identification of the high-velocity Ivrea body, which altogether leads to a spatially more complete 3-D crustal model in the western Alpine region.

The high consistency between our new 3-D crustal model and the LET model of Diehl *et al.* (2009a) in terms of Moho topography (Fig. 10b) indicates improvements compared to the model of Husen *et al.* (2003). This is mainly attributed to our approach of combining data from both CSS and LET methods in an approximated coupled inversion instead of using CSS results as *a priori* constraints for the inversion of LET data.

In addition, our model is also more complete and better than the existing 3-D CSS velocity model of Waldhauser *et al.* (2002) that aimed at correcting the crustal influence on teleseismic travel-times (Lippitsch *et al.* 2003). In contrast to our 3-D crustal model,

in their study the Ivrea body, for example, was only *a posteriori* included into their model based on results of Solarino *et al.* (1997). Thus, the new procedure presented in this study for combining CSS and LET Moho information denotes the first and most important step towards such a reference 3-D crustal model. Following a similar approach as Waldhauser *et al.* (2002) and including crustal velocities of the LET model of Diehl *et al.* (2009a) with their velocity gradients adapted to the new combined CSS and LET Moho topography represents the best and most complete initial 3-D crustal model. When complemented with hopefully soon available *S*-wave information, such a detailed reference 3-D velocity model will also be highly suitable for earthquake source parameter determinations that then can make use of strong secondary phases resulting from seismic wave interactions at the Moho discontinuity.
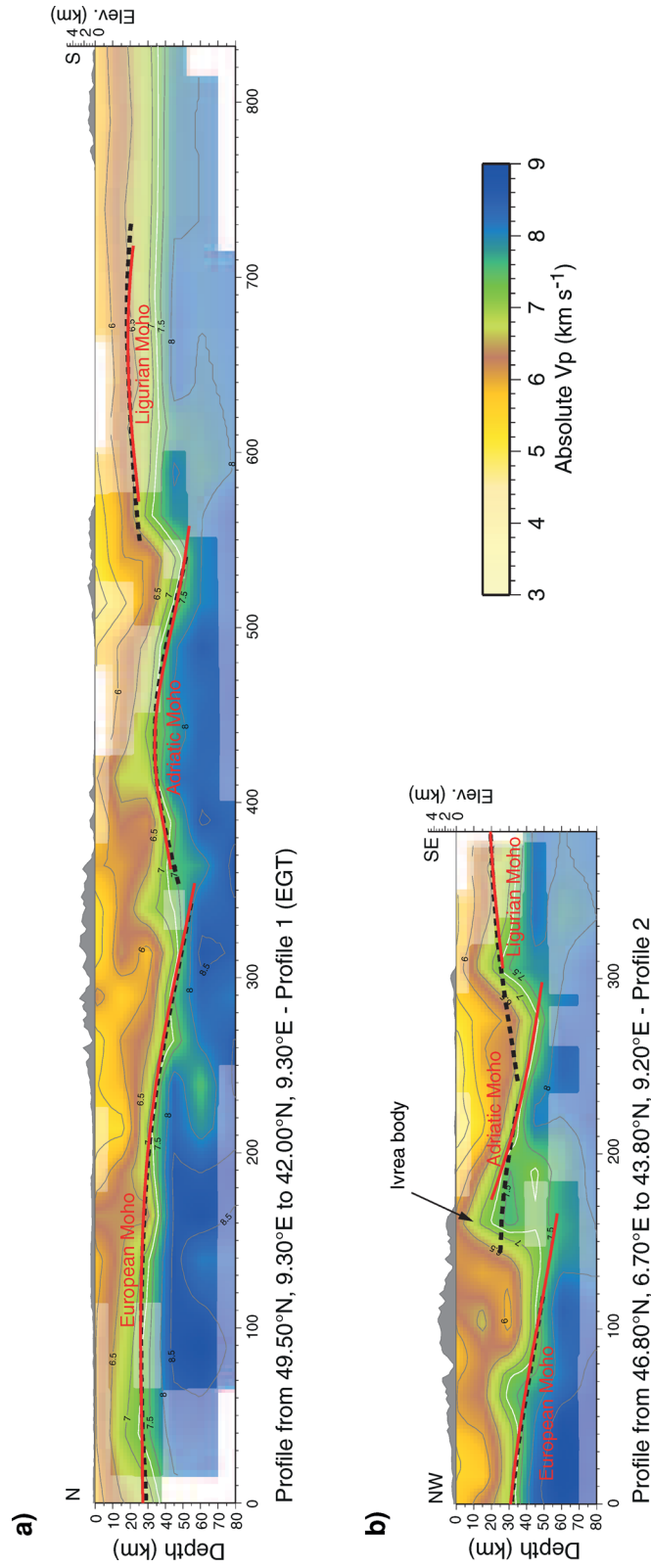
Figure 9. Vertical cross-sections through 3-D LET model of Diehl *et al.* (2009a). For orientation of profiles see Fig. 8. Thin white contour line of 7.25 km s⁻¹ velocity approximately marks the LET-derived Moho. Dashed black line marks the CSS-only-derived Moho topography of Waldhauser *et al.* (1998). Thick red line shows the Moho depth of our improved 3-D crustal model. (a, b) Note the good correlation of previous and new Moho topography where sufficient CSS data of high quality were available (e.g. along Profile 1) and significant improvements in Moho topography across plate boundaries where original CSS data were insufficient (e.g. along Profile 2). Shaded colours outline areas of insufficient resolution. Areas with very poor ray coverage are shown in white.
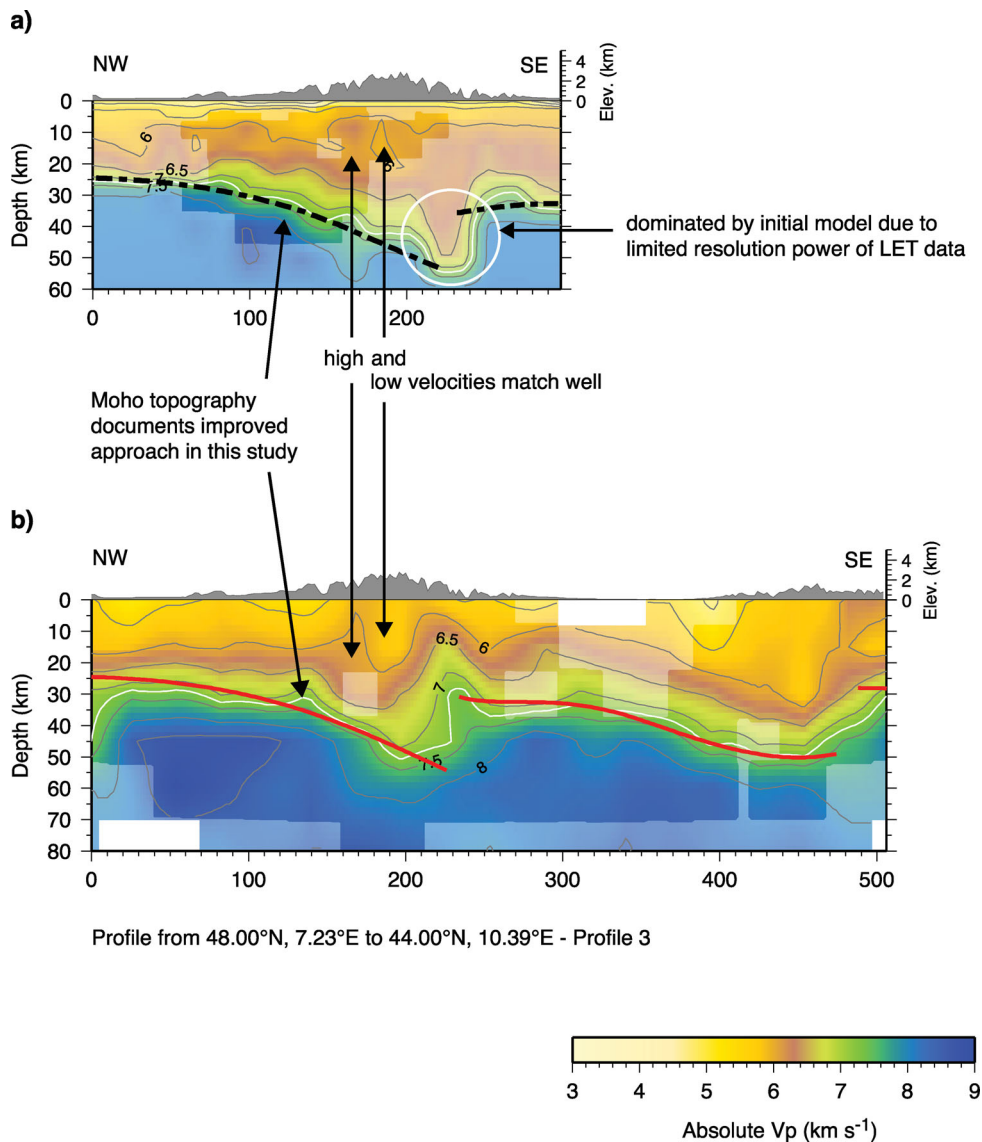
Figure 10. (a) Vertical cross-section through 3-D LET model of Husen *et al.* (2003). Thin white contour line marks 7.25 km s^{-1} velocity. Dashed black line shows Moho depth after Waldhauser *et al.* (1998). Area marked by white circle and the shape of 7.25 km s^{-1} isoline in the left and middle part of the profile show the limited resolution power of LET data at greater depths and the influence of the starting model. Shaded colours outline areas of insufficient resolution. (b) Vertical cross-section through 3-D LET model of Diehl *et al.* (2009a). Thin white contour line marks 7.25 km s^{-1} velocity. Thick red line shows the Moho depth of our improved 3-D crustal model. Shaded colours outline areas of insufficient resolution. Areas with very poor ray coverage are shown in white. For orientation of profiles see Fig. 8.

REFERENCES

Aldersons, F., 2004. Toward three-dimensional crustal structure of the Dead Sea region from local earthquake tomography, *PhD thesis*, Tel Aviv University, Israel.

Ansorge, J. & Baumann, M., 1997. Acquisition of seismic refraction data within NFP20 (Switzerland), in *Deep Structure of the Swiss Alps: Results of NRP20,* pp. 25–30, Birkhäuser Verlag, Basel.

Banda, E. & Mooney, W.D., 1982. Present and future trends in controlled source seismology: a partial view, *Terra Cognita,* **2**(4), 355–362.

Baumann, M., 1994. Three-dimensional modeling of the crust-mantle boundary in the Alpine region, *PhD thesis*, Swiss Federal Institute of Technology Zurich.

Béthoux, N., Sue, C., Paul, A., Virieux, J., Fréchet, J., Thouvenot, F. & Cattaneo, M., 2007. Local tomography and focal mechanisms in the south-western Alps: comparison of methods and tectonic implications, *Tectonophysics,* **432**(1–4), 1–19.

Blundell, D., Freeman, R. & Mueller, S., 1992. *A Continent Revealed, the European Geotraverse,* Cambridge University Press, New York.

Christensen, N., 1996. Poisson's ratio and crustal seismology, *J. geophys. Res.,* **101**(B2), 3139–3156.

Di Stefano, R., Aldersons, F., Kissling, E., Baccheschi, P., Chiarabba, C. & Giardini, D., 2006. Automatic seismic phase picking and consistent observation error assessment: application to the Italian seismicity, *Geophys. J. Int.,* **165**(1), 121–134.

Di Stefano, R., Kissling, E., Chiarabba, C., Amato, A. & Giardini, D., 2009. Shallow subduction beneath Italy: three-dimensional images of the Adriatic-European-Tyrrhenian lithosphere system based on high-quality P wave arrival times, *J. geophys. Res.,* **114**(B5), 1–17.

Di Stefano, R., Bianchi, I., Ciaccio, M.G., Carrara, G. & Kissling, E., 2011. Three-dimensional Moho topography in Italy: new constraints from receiver functions and controlled source seismology, *Geochemist. Geophys. Geosystems.,* **12**(9), 1–15.

Diehl, T., Husen, S., Kissling, E. & Deichmann, N., 2009a. High-resolution 3-D P-wave model of the Alpine crust, *Geophys. J. Int.,* **179**(2), 1133–1147.

Diehl, T., Kissling, E., Husen, S. & Aldersons, F., 2009b. Consistent phase picking for regional tomography models: application to the greater Alpine region, *Geophys. J. Int.,* **176**(2), 542–554.

Eberhart-Phillips, D., 1990. Three-dimensional P and S velocity structure in the Coalinga Region, California, *J. geophys. Res.,* **95**(B10), 15 315–343 363.

Eberhart-Phillips, D., 1993. Local earthquake tomography: earthquake source regions, in *Seismic Tomography: Theory and Practice,* eds Iyer, H.M. & Hirahara, K., Chapman & Hall, London.

Haslinger, F. *et al.,* 1999. 3D crustal structure from local earthquake tomography around the Gulf of Arta (Ionian region, NW Greece), *Tectonophysics,* **304**(3), 201–218.

Holliger, K. & Kissling, E., 1991. Ray theoretical depth migration: methodology and application to deep seismic-reflection data across the eastern and southern Swiss-Alps, *Eclogae Geol. Helv.,* **84**(2), 369–402.

Husen, S., Kissling, E. & Flueh, E.R., 2000. Local earthquake tomography of shallow subduction in north Chile: a combined onshore and offshore study, *J. geophys. Res.,* **105**(B12), 28 183–28 198.

Husen, S., Kissling, E., Deichmann, N., Wiemer, S., Giardini, D. & Baer, M., 2003. Probabilistic earthquake location in complex three-dimensional velocity models: application to Switzerland, *J. geophys. Res.,* **108**(B2), 2077, doi:10.1029/2002JB001778.

Kissling, E., 1988. Geotomography with local earthquake data, *Rev. Geophys.,* **26**(4), 659–698.

Kissling, E., 1993. Deep structure of the Alps: what do we really know? *Phys. Earth planet. Inter.,* **79**(1–2), 87–112.

Kissling, E. & Husen, S., 2001. Model parametrization in seismic tomography: a choice of consequence for the solution quality, *Phys. Earth planet. Inter.,* **123**(2–4), 89–101.

Kissling, E., Ellsworth, W., Eberhart-Phillips, D. & Kradolfer, U., 1994. Initial reference models in local earthquake tomography, *J. geophys. Res.,* **99,** 19, 635–19, 646.

Kissling, E., Ansorge, J. & Baumann, M., 1997. Methodological considerations of 3-D crustal structure modeling by 2-D seimic methods, in *Deep Structure of Switzerland,* pp. 31–38, eds Heitzmann, P., Pfiffner, O., Lehner, P., Mueller, S. & Steck, A., Birkhaeuser, Verlag, Basel.

Kissling, E., Schmid, S., Lippitsch, R., Ansorge, J. & Fügenschuh, B., 2006. Lithosphere structure and tectonic evolution of the Alpine arc: new evidence from high-resolution teleseismic tomography, *Geol. Soc., Lond., Memoirs,* **32**(1), 129–145.

Lippitsch, R., Kissling, E. & Ansorge, J., 2003. Upper mantle structure beneath the Alpine orogen from high-resolution teleseismic tomography, *J. geophys. Res.,* **108**(B8), 2376, doi:10.1029/2002JB002016.

Miller, D. & Smith, R., 1999. P and S velocity structure of the Yellowstone volcanic field from local earthquake and controlled-source tomography, *J. geophys. Res.,* **104**(B7), 15105–15121.

Mooney, W.D., Laske, G. & Masters, T.G., 1998. CRUST 5.1: A global crustal model at 5° x 5°, *J. geophys. Res.,* **103**(B1), 727–747.

Mueller, S., 1977. A new model of the continental crust, in *The Earth's Crust,* Vol. 20, pp. 727–747, Geophysical Monograph, Am. Geophys. Union.

Reyners, M., Eberhart-Phillips, D. & Stuart, G., 1999. A three-dimensional image of shallow subduction: crustal structure of the Raukumara Peninsula, New Zealand, *Geophys. J. Int.,* **137**(3), 873–890.

Schmid, R., 1967. Zur Petrographie und Struktur der Zone Ivrea-Verbano zwischen Valle d'Ossola und Val Grande (Prov. Novara, Italien), *Schweizer. Min. Petr. Mitt.,* **47**, 935–1117.

Schmid, R., 1968. Excursion guide for the Valle d'Ossola section of the Ivrea-Verbano Zone (Geologische Uebersichtsskizze der Gegend nordwestlich des Lago Maggiore), *Schweizer. Min. Petr. Mitt.,* **48**, 305–313.

Schmid, S.M. & Kissling, E., 2000. The arc of the western Alps in the light of geophysical data on deep crustal structure, *Tectonics,* **19**(1), 62–85.

Schmid, S.M., Fügenschuh, B., Kissling, E. & Schuster, R., 2004. Tectonic map and overall architecture of the Alpine orogen, *Eclogae Geologicae Helvetiae,* **97**(1), 93–117.

Solarino, S., Kissling, E., Sellami, S., Smriglio, G., Thouvenot, F., Granet, M., Bonjer, K. & Slejko, D., 1997. Compilation of a recent seismicity data base of the greater Alpine region from several seismological networks and preliminary 3D tomographic results, *Ann. Geophys.,* **40**(1), 161–174.

Thurber, C., 1983. Earthquake location and three-dimensional crustal structure in the Coyote lake area, Central California, *J. geophys. Res.,* **88**, 8226–8236.

Waldhauser, F., 1996. A parameterized three-dimensional Alpine crustal model and its application to teleseismic wavefront scattering, *PhD thesis,* Swiss Federal Institute of Technology Zurich.

Waldhauser, F., Kissling, E., Ansorge, J. & Mueller, S., 1998. Three-dimensional interface modelling with two-dimensional seismic data: the Alpine crust-mantle boundary, *Geophys. J. Int.,* **135**(1), 264–278.

Waldhauser, F., Lippitsch, R., Kissling, E. & Ansorge, J., 2002. High-resolution teleseismic tomography of upper-mantle structure using an a priori three-dimensional crustal model, *Geophys. J. Int.,* **150**(2), 403–414.

Wessel, P. & Smith, W.H.F., 1998. New, improved version of the Generic Mapping Tools released, *EOS, Trans. Am. geophys. Un.,* **79**(47), 579, doi:10.1029/98E000926.

APPENDIX A: ADDITIONAL INFORMATION ON 'CONSISTENCY IN CSS AND LET MOHO DATA'

Vertical cross-sections through the 3-D LET *P*-wave velocity model showing CSS and LET Moho elements as well as the respective interpolated CSS and LET Moho (Figs 3b and c) are useful to assess the reasons for similarities and differences in CSS and LET Moho depths.

Local Moho topography and weak LET velocity gradients

In some parts of the LET model with good resolution local LET Moho topography can be seen where CSS data indicate a rather smooth topography (Fig. 3b). As mentioned in Section 2.1 this is due to the sparsity of CSS data in these regions and the principle of interface simplicity. As a consequence, the CSS model will represent the smoothest and simplest Moho interface that still fits the data and has the highest continuity (Waldhauser *et al.* 1998). Thus, if real Moho topography is poorly sampled in space, modelled Moho topography is too smooth. A weak velocity gradient in LET results in rejection of LET Moho information (Fig. 3b).

Moho offsets, plate boundaries and Ivrea body

At Moho offsets and other plate boundaries of complex velocity structure, it is not always easy to allocate reflector elements with the correct Moho surface (see Appendix B). Furthermore, in these areas 3-D migration of CSS Moho reflector elements is likely ambiguous and strongly dependent on the local velocity structure. Due to the source-receiver geometry of CSS methods, the narrow sub-vertical Ivrea body with its high velocities is not directly 'visible' by CSS experiments (e.g. Kissling 1993). Hence, in Waldhauser *et al.* (1998, 2002) no Ivrea information was available for the 3-D migration of CSS Moho reflector elements leading to some grossly misplaced CSS Moho reflectors in the vicinity of the Ivrea body (Figs 3c and 4).

In this study, however, 3-D migration of all CSS reflector elements is based on a new surface for migration for which LET Moho elements and, therefore, the Ivrea body's geometry are considered.

APPENDIX B: AUTOMATED ASSOCIATION OF LET MOHO ELEMENTS WITH MOHO SURFACES

After the automated definition of each LET Moho element's depth, it individually needs to be associated with a Moho surface, being Europe, Adria or Liguria (Waldhauser *et al.* 1998). This procedure is analogous to the association of CSS Moho data with a Moho surface. Hence, association with a Moho surface must be based on *a priori* defined areas (polygons) for each Moho surface. In a first step these *a priori* defined Moho polygons are related to the ones used by Waldhauser *et al.* (1998) for CSS data only. Near plate boundaries, association of Moho elements is somewhat ambiguous. Therefore, automated association is only applied within zones defined by polygons that remain at least a distance of 20 km from plate boundaries (Fig. 4). All LET Moho elements outside these polygonal areas defining the three Moho surfaces must be manually checked and associated. This is realized with the help of several cross-sections through the LET model of Diehl *et al.* (2009a) across each plate boundary.

APPENDIX C: MANUAL EXTRACTION AND ASSOCIATION OF LET MOHO ELEMENTS

When an automated extraction of LET Moho elements is not possible (see above), manual extraction and association might still be applicable. In general, the procedure is the same as it is in the automated case, but now the criteria for identification of LET Moho elements (Table 1) are applied differently. In addition to the normal approach of considering the vertical velocity gradient, it proves useful to take into account the velocity gradient in horizontal directions for some special cases as well. It is, for example, useful at the very steep western end of the Ivrea body, where a strong horizontal velocity gradient prevails (see Figs 3c and 5). In such cases where a significant vertical Moho offset exists, one may follow the 7.25 km s^{-1} contour line while tracking the velocity gradient across the Moho from either plate as far as possible to identify the Moho depths and location of the Moho offset (Fig. 5). While manual extraction and association of LET Moho elements in principle is straightforward, corresponding estimates of uncertainties remain somewhat ambiguous in relation to automatically extracted Moho depths. Therefore, uncertainties of all manually obtained Moho elements are uniformly set to ±15 km, that is, the lowest possible quality used for Moho interpolation.